

# Atomic Scale Dynamics of Contact Formation in the Cross-Section of InGaAs Nanowire Channels

Renjie Chen,<sup>†</sup> Katherine L. Jungjohann,<sup>‡</sup> William M. Mook,<sup>‡</sup> John Nogan,<sup>‡</sup> and Shadi A. Dayeh<sup>\*,†,§,||</sup>

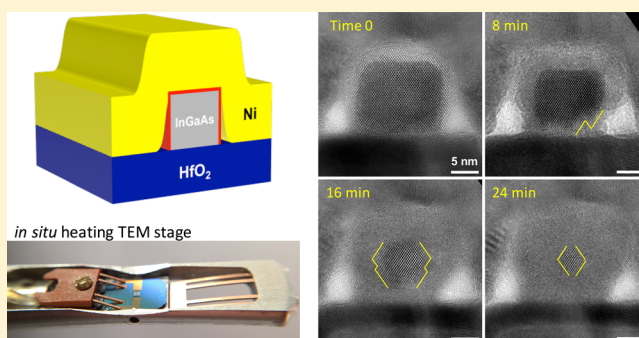
<sup>†</sup>Department of Electrical and Computer Engineering, <sup>§</sup>Materials Science and Engineering Program, <sup>||</sup>Department of NanoEngineering, University of California San Diego, La Jolla, California 92093, United States

<sup>‡</sup>Center for Integrated Nanotechnologies, Sandia National Laboratories, Albuquerque, New Mexico 87185, United States

## Supporting Information

**ABSTRACT:** Alloyed and compound contacts between metal and semiconductor transistor channels enable self-aligned gate processes which play a significant role in transistor scaling. At nanoscale dimensions and for nanowire channels, prior experiments focused on reactions along the channel length, but the early stage of reaction in their cross sections remains unknown. Here, we report on the dynamics of the solid-state reaction between metal (Ni) and semiconductor ( $\text{In}_{0.53}\text{Ga}_{0.47}\text{As}$ ), along the cross-section of nanowires that are 15 nm in width. Unlike planar structures where crystalline nickelide readily forms at conventional, low alloying temperatures, nanowires exhibit a solid-state amorphization step that can undergo a crystal regrowth step at elevated temperatures. In this study, we capture the layer-by-layer reaction mechanism and growth rate anisotropy using in situ transmission electron microscopy (TEM). Our kinetic model depicts this new, in-plane contact formation which could pave the way for engineered nanoscale transistors.

**KEYWORDS:** *In situ TEM, InGaAs, nanowire, nickelide, amorphization, recrystallization*



The metal–semiconductor contact in ultrascaled devices is one of the most critical factors limiting device performance, especially in the world of “smaller is better”,<sup>1</sup> where nanowires<sup>2–4</sup> and high aspect ratio rectangular channels known as Fins<sup>5–7</sup> excel. Alloyed contacts, formed by thermal annealing of metal–semiconductor nanowires, are prescribed for lithography-free self-aligned gate design.<sup>8,9</sup> The advent of semiconductor nanowires evoked reevaluation of the thermodynamics,<sup>10</sup> kinetics,<sup>11,12</sup> and phases<sup>13,14</sup> in nanoscale metal–semiconductor reactions, which deviate significantly from the behaviors exhibited by their planar counterparts. These efforts captured the evolution of the reaction along the axis of the nanoscale channel,<sup>15–17</sup> but the early stage of the reaction under the metal contact in the radial direction of the nanowire’s cross-section is critical and has not been studied until now. From a materials perspective, the early stage of the reaction can govern the channel’s final phases and crystalline orientations once the reaction extends into the horizontal segment (forming an end-bond-contact geometry) and can be largely affected by local defects<sup>18</sup> or interfacial properties. From an engineering perspective, the early stage reaction facilitates a side-contact geometry in nanowire devices that is more desirable for self-aligned technology than an end-bond-contact geometry. These issues demand a detailed understanding of the early stage reaction along the nanowire’s cross-section.

Here, we focus on the narrow band gap, high electron mobility III–V semiconductor,  $\text{In}_x\text{Ga}_{1-x}\text{As}$ , motivated by its

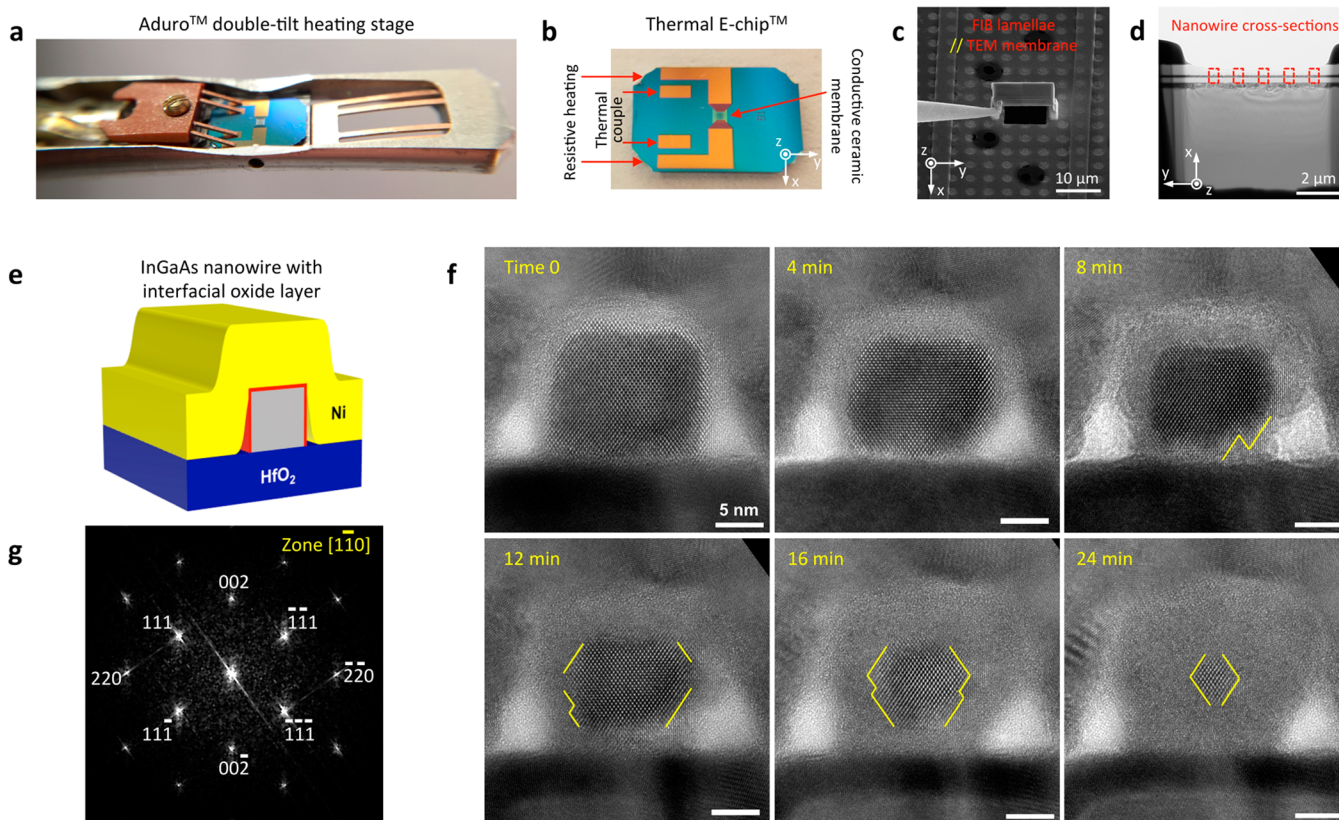
potential in sub-10 nm metal–oxide–semiconductor field-effect transistors (MOSFETs).<sup>1</sup> Ni permits superior metal contacts to  $\text{In}_{0.53}\text{Ga}_{0.47}\text{As}$  devices<sup>19</sup> by diffusing into  $\text{In}_{0.53}\text{Ga}_{0.47}\text{As}$  and forming a metallic nickelide ( $\text{Ni}_x\text{In}_{0.53}\text{Ga}_{0.47}\text{As}$ ) phase through a solid-state reaction,<sup>20–22</sup> analogous to the nickel silicide ( $\text{Ni}_x\text{Si}$ ) to Si devices. In planar device geometries, the nickelide reaction starts at  $\sim 230$  °C, and the polycrystalline phase is thermally stable up to 450 °C.<sup>23</sup> The  $\text{Ni}_x\text{In}_{0.53}\text{Ga}_{0.47}\text{As}$  lattice adopts the NiAs (B8) structure with  $x = 2$  ( $\text{Ni}_2\text{In}_{0.53}\text{Ga}_{0.47}\text{As}$ ).<sup>24–26</sup> However, in nanowire structures, the reaction dynamics and formed phases are yet to be understood. Herein, we perform in situ TEM heating experiments to characterize the solid-state reaction between Ni and the  $\text{In}_{0.53}\text{Ga}_{0.47}\text{As}$  nanowire along its cross-section.

Figure 1a–b shows the in situ heating stage and the compatible thermal E-chip that has a thin membrane window for placing our specimen. Temperatures are controlled by resistive heating and are continuously measured on-chip with a thermocouple. Samples that have Ni contacts on  $\text{In}_{0.53}\text{Ga}_{0.47}\text{As}$  nanowires were fabricated on a separate substrate and transferred on top of the membrane window of a thermal E-chip by focused-ion-beam (FIB) milling via the lift-out procedure (see section I of Supporting Information, SI). In

**Received:** November 10, 2016

**Revised:** February 24, 2017

**Published:** March 23, 2017



**Figure 1.** In situ heating TEM platform and reaction dynamics. (a–b) photographs of the Protochips Aduro heating stage and its compatible thermal E-chip, respectively. Four probes on the heating stage contact the metal leads on the thermal E-chip to introduce resistive heating and to read out temperatures. (c) SEM image of the FIB milled specimen lamellae transferred horizontally onto the TEM membrane of the thermal E-chip. (d) TEM image showing an overview of the specimen lamellae and the labeled locations of nanowire cross-sections. (e) Schematic of Ni contacting with a  $\text{In}_{0.53}\text{Ga}_{0.47}\text{As}$  nanowire cross-section that sits on the  $\text{HfO}_2$  dielectric layer. A thin red layer indicates the intentionally introduced  $\text{In}_{0.53}\text{Ga}_{0.47}\text{As}$  surface oxide layer before Ni deposition. (f) HRTEM sequences extracted from [Movie S1](#) in the SI during the in situ heating experiment at  $180^\circ\text{C}$ . During this process, Ni diffuses through the interfacial oxide layer, reacts with the  $\text{In}_{0.53}\text{Ga}_{0.47}\text{As}$  nanowire channel, and results in an amorphous nickelide phase. The nanowire cross-section, started with straight sidewalls, became initially rounded and gradually developed facets with a diamond shape. (g) Fast Fourier transform (FFT) image of the corresponding nanowire cross-section, showing the diffraction pattern along the  $[1\bar{1}0]$  zone axis (projecting direction in TEM). The developed facets in panel f correspond to the  $\{111\}$  type of facets for  $\text{In}_{0.53}\text{Ga}_{0.47}\text{As}$  lattice that has a zinc blende structure.

the first set of in situ heating experiments, we chose a specimen that had a thin (1–2 nm) surface oxide layer in between the Ni contact and  $\text{In}_{0.53}\text{Ga}_{0.47}\text{As}$  nanowire ([Figure 1e](#)). This was to prevent the intermixing<sup>27</sup> between Ni and  $\text{In}_{0.53}\text{Ga}_{0.47}\text{As}$  nanowire upon Ni deposition ([Figure S1](#), SI). The as-fabricated  $\text{In}_{0.53}\text{Ga}_{0.47}\text{As}$  nanowire had a square cross-section with an edge width of  $\sim 15$  nm. At temperatures above  $180^\circ\text{C}$ , Ni diffused through the interfacial oxide layer and reacted with the  $\text{In}_{0.53}\text{Ga}_{0.47}\text{As}$  nanowire cross-section to form an amorphous nickelide ( $\text{Ni}_x\text{In}_{0.53}\text{Ga}_{0.47}\text{As}$ ) phase. This is significantly different from the planar case, as the temperature at which the reaction started was reduced by  $\sim 50^\circ\text{C}$  and the nickelide phase was amorphous rather than the crystalline  $\text{Ni}_2\text{In}_{0.53}\text{Ga}_{0.47}\text{As}$  that is usually obtained at or above  $230^\circ\text{C}$  ([Figure S5](#), SI).

To capture the details of this solid-state amorphization process, we recorded the atomic-resolution sequence at  $180^\circ\text{C}$  ([Figure 1f](#)). At the onset of the reaction, the Ni diffused through the interfacial oxide layer and along the surface of  $\text{In}_{0.53}\text{Ga}_{0.47}\text{As}$  nanowire, quickly forming an amorphous nickelide shell of uniform thickness. Then, the nickelide shell grew evenly along the top and side surfaces of the nanowire ([Figure 1f](#),  $t = 4$  min), even in regions without intimate contact between Ni and the nanowire sidewall (due to shadowing effects in the

metal deposition process). The growth of the surface nickelide shell indicated that surface-diffusion of Ni atoms along the outer few atomic layers of the  $\text{In}_{0.53}\text{Ga}_{0.47}\text{As}$  nanowire is much faster than the volume-diffusion rate when Ni diffuses further into the nanowire cross-section.<sup>28</sup> Following this shell formation ([Figure 1f](#),  $t = 8$  min), the nickelide reaction continued along the bottom region of the nanowire that sits on  $\text{HfO}_2$  and then extended across the width of the nanowire isolating the crystalline  $\text{In}_{0.53}\text{Ga}_{0.47}\text{As}$  core from the  $\text{HfO}_2$  substrate ([Figure 1f](#),  $t = 12$  min) by an intermediate amorphous nickelide region. This process led to the formation of an isotropic nickelide shell surrounding the entire  $\text{InGaAs}$  nanowire circumference. At this point the  $(110)$  sidewall facets start to disappear by developing multiple  $\{111\}$ -type facets, while the top facet remains  $(001)$ , indicating a faster reaction rate on  $\{110\}$  compared to  $\{111\}$  and  $\{001\}$  surfaces. This process created a stepped interface ([Figure 2](#)) that was gradually eliminated by  $\{111\}$  facets resulting in a rhomboidal core of crystalline  $\text{In}_{0.53}\text{Ga}_{0.47}\text{As}$  ([Figure 1f](#),  $t = 24$  min).

The details of the facet evolution and ledge movement are revealed in the still images of the high-resolution TEM recording ([Figure 2a](#)) with much shorter time intervals in the time range of 12–16 min shown in [Figure 1f](#). We observed

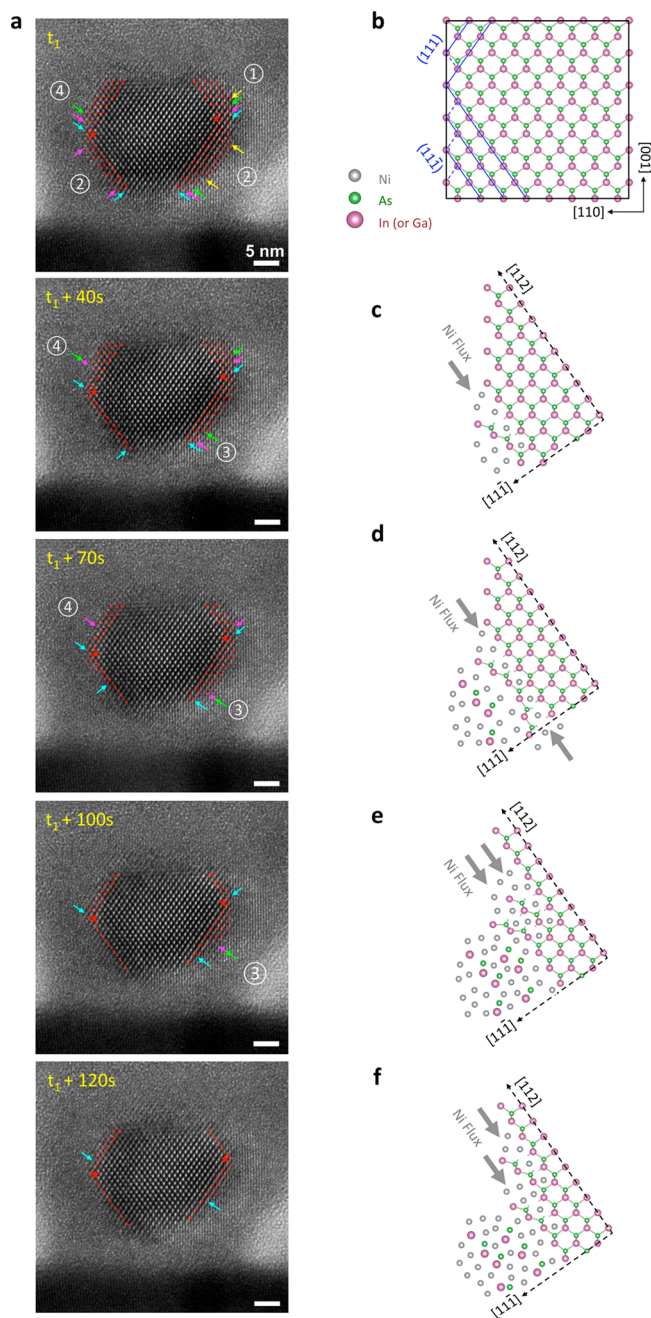


**Figure 2.** Ledge formation and movement mechanisms at atomic resolution. (a) HRTEM sequences extracted from shorter time duration in *Movie S1* in the SI showing the evolution of  $\{110\}$  sidewall facet into multiple  $\{111\}$  type facets, through the layer-by-layer nickelide reactions. Red stars label the identical atoms in each figure. (b) Reconstructed  $\text{In}_x\text{Ga}_{1-x}\text{As}$  lattice structure with the same orientation as the nanowire cross-section. (c–f) Proposed mechanism of ledge movement on  $(11\bar{1})$  plane along  $[112]$  or  $[\bar{1}12]$  directions. The ledge can move with a step height of one  $\text{In}_x\text{Ga}_{1-x}\text{As}$  bilayer, from one side (c) or two opposite sides (d) corresponding to the labeled cases of ① and ② in panel a. The ledge can also move with a step height of two  $\text{In}_x\text{Ga}_{1-x}\text{As}$  bilayers together (e) and can separate into two single bilayers afterward (f) which corresponds to the labeled cases of ③ and ④ in panel a.

layer-by-layer Ni reactions on  $\{111\}$  facets with ledge movements that can be characterized by one of the following mechanisms: (1) a step height that eliminates one  $\text{In}_{0.53}\text{Ga}_{0.47}\text{As}$  atomic bilayer<sup>29</sup> along a single  $\langle 112 \rangle$  direction (labeled ① in

Figure 2a and shown in the schematic of Figure 2c), (2) a step height that eliminates one atomic bilayer but with the reaction proceeding from both sides of the bilayer in two opposite  $\langle 112 \rangle$  directions (labeled ② in Figure 2a and shown in the schematic of Figure 2d), (3) the merging of two ledges, each with a single-bilayer step height, into a single ledge with a double-bilayer step height (labeled ③ in Figure 2a and shown in the schematic of Figure 2f) that moves simultaneously after merging, or (4) the split of a double-bilayer step height into two ledges with single-bilayer step heights (labeled ④ in Figure 2a and shown in the schematic of Figure 2e) that moves independently after splitting. These observations imply that there was no shear stress during this nickelide reaction in our current device geometry because a fixed step height of three or more atomic bilayers is necessary in order to compensate for the shear stress during phase transformations,<sup>30</sup> which was not observed in our experiments. Therefore, we believe that these four possible scenarios of ledge movement are general to the Ni/III–V nanowire reaction. We emphasize that Figure 2 not only correlates the nature of ledge movements to the crystal structures in the nanowire cross-section but also tracks the time-resolved amorphization reaction in III–V materials at atomic resolution.

The general behavior of the phase transformation in the nanowire cross-section that is exhibited in Figure 2 is valid with or without the presence of the interfacial oxide. The direct deposition of metal on a compound semiconductor surface leads to the formation of an intermixing layer due to the latent heat when the metal atoms condense from the vapor phase to the solid phase.<sup>27</sup> Irrespective of the deposition process (electron beam evaporation or sputtering), we determined that, prior to the in situ heating experiments, our devices exhibited a Ni– $\text{In}_{0.53}\text{Ga}_{0.47}\text{As}$  intermixing surface layer for those that did not have a surface oxide layer (Figure 3a). Ion-beam irradiation intermixing during TEM sample preparation was tested and excluded as being a cause for this behavior (see section II and Figure S4 of SI). We observed that, before the in situ heating experiment started, the  $\text{In}_{0.53}\text{Ga}_{0.47}\text{As}$  core had a rounded top and sidewall surfaces (Figure 3b,  $t = 0$ ) due to the formation of the intermixing layer. When heated to 180 °C, Ni diffused through the existing intermixing layer, along the rounded surface of crystalline  $\text{In}_{0.53}\text{Ga}_{0.47}\text{As}$ , and reacted at the interface between  $\text{In}_{0.53}\text{Ga}_{0.47}\text{As}$  and  $\text{HfO}_2$  at the bottom of the nanowire, making the  $\text{In}_{0.53}\text{Ga}_{0.47}\text{As}$  core even more rounded (Figure 3b,  $t = 3$  min). As the reaction progressed, many small facets were clearly observed at 6 min and gradually developed into several  $\{111\}$  type of facets at 9 min. Eventually, the crystalline  $\text{In}_{0.53}\text{Ga}_{0.47}\text{As}$  core became a rhomboidal shape after 13 min, very similar to that of Figure 1f with the only difference being the relatively lower spatial position of the rhombus due to the initial intermixing layer.

In order to better understand the kinetics and thermodynamics of the nickelide reaction in the radial direction of the nanowire's cross-section, we developed a simple model (Figure 4a) to depict this metallization process. For simplicity, we assumed that (i) the metal contact was an infinite source of Ni since there was no experimentally observed depletion of Ni near the nickelide/nanowire interface; (ii) the unreacted semiconductor core and reacted metallic shell were cylindrical with perimeters,  $l$  and  $L$ , respectively; and (iii)  $L$  was fixed which is consistent with our experimental observations in Figure 4b–c. The fixed perimeter  $L$  suggests that the volume expansion due to Ni incorporation occurred in the  $h$  direction,

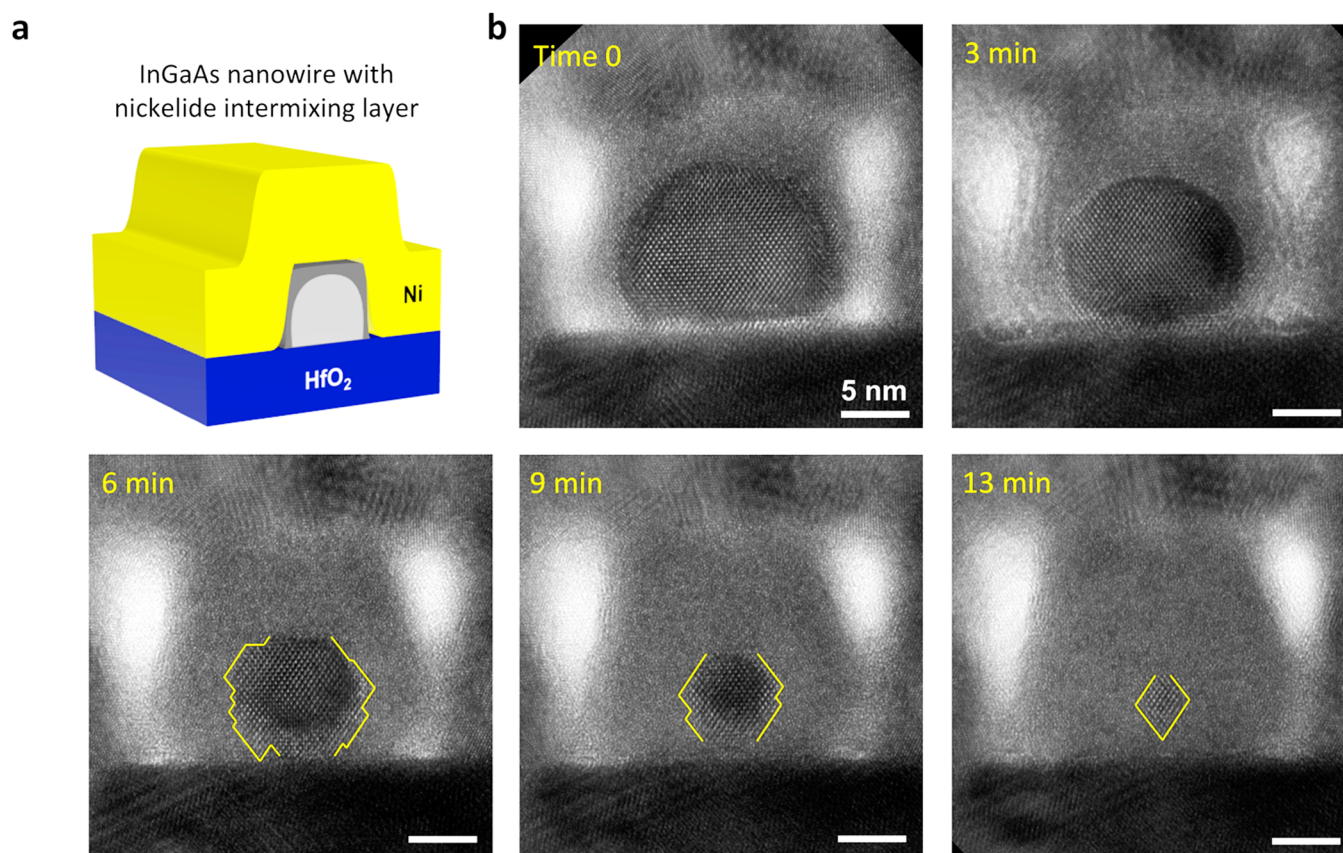


**Figure 3.** Influence of nickelide intermixing layer. (a) Schematic of Ni contacting with a  $\text{In}_{0.53}\text{Ga}_{0.47}\text{As}$  nanowire cross-section without the introduced oxide interface. An amorphous intermixing layer readily forms upon Ni deposition. (b) High-resolution TEM sequences extracted from [Movie S2](#) in the SI during the in situ heating at  $180\text{ }^\circ\text{C}$ . The nonintermixed  $\text{In}_{0.53}\text{Ga}_{0.47}\text{As}$  cross-section, started with rounded structure and gradually developed multiple small facets/steps as highlighted by the yellow lines for  $t = 6$  min onward, finally forming an equilateral rhombus-like region.

and negligible strain was present in the  $\text{In}_{0.53}\text{Ga}_{0.47}\text{As}$  core for the present experimental conditions, as was validated from fast Fourier transform (FFT) patterns on the InGaAs regions at various stages of the reaction.

As shown in [Figure 4a](#), the mass transport of Ni atoms in the nickelide reaction involves three steps: (1) Ni dissolution across the Ni/nickelide interface, (2) Ni diffusion through the formed nickelide shell, and (3) solid-state reaction at the nickelide/ $\text{In}_{0.53}\text{Ga}_{0.47}\text{As}$  interface, with Ni fluxes denoted as  $F_1$ ,  $F_2$ , and  $F_3$ , respectively. If one of the three steps is the rate-limiting step, the correlation between the unreacted perimeter  $l$  and time  $t$  can be expressed as follows (section III, [SI](#)):

(i) If  $F_1$  is the rate-limiting step:

$$l(t) = \sqrt{L^2 - 2k_{\text{dissolve}}LPt} \quad (1)$$

(ii) If  $F_2$  is the rate-limiting step:

$$2l(t)^2 \ln(l(t)/L) + L^2 - l(t)^2 = 8\pi D_{\text{Ni}}Pt \quad (2)$$

(iii) If  $F_3$  is the rate-limiting step:

$$l(t) = L - k_{\text{growth}}Pt \quad (3)$$

where  $k_{\text{dissolve}}$  and  $k_{\text{growth}}$  are the rate constants for Ni dissolution and nickelide growth, respectively.  $D_{\text{Ni}}$  is the diffusion coefficient of Ni in  $\text{In}_{0.53}\text{Ga}_{0.47}\text{As}$ , and  $P$  is a constant.

We found that for the first type of specimen that had an interfacial oxide layer in between Ni and  $\text{In}_{0.53}\text{Ga}_{0.47}\text{As}$  ([Figures 1 and 2](#)),  $l$  obeyed a linear dependence on time ([Figure 4b](#)) that

follows [eq 3](#), a behavior that is consistent with  $F_3$  being the rate-limiting step, i.e., kinetically limited growth at the nickelide/ $\text{In}_{0.53}\text{Ga}_{0.47}\text{As}$  interface. By fitting the experimental data in [Figure 4b](#) to [eq 3](#), we found that the fit line projected to an intercept,  $L$ , of  $64.2\text{ nm}$  with the  $y$ -axis, which is in agreement with the external nickelide perimeter within the measurement errors. The slope of the linear fit provided the effective growth rate ( $k_{\text{growth}}P$ ) of  $2.1\text{ nm/min}$ . Since Ni mainly reacted with three surfaces with the nanowire cross-section but not at the  $\text{In}_{0.53}\text{Ga}_{0.47}\text{As}/\text{HfO}_2$  lower interface for the first 8 min of the reaction, the experimentally extracted reacted perimeter is lower than the modeled one in [Figure 4b](#). For the second type of specimen that had the intermixing layer in between Ni and  $\text{In}_{0.53}\text{Ga}_{0.47}\text{As}$  ([Figure 4c](#)),  $l$  followed a diffusion/mass-transport-limited process ( $F_2$ ) with a characteristic dependence of [eq 2](#). The characteristic shape of [eq 2](#) includes rapid decays in unreacted perimeter  $l$  at both the beginning and the very end and an approximate linear segment in between. The fit to the data of [Figure 4c](#) with [eq 2](#) included a time-offset term  $(t - t_0)$ , where  $t_0 = 1.9\text{ min}$ , indicating that the diffusion-limited growth rate became effective after  $\sim 2$  min of reaction. This behavior raises two questions: why did the reaction rate in the second type of specimen change from kinetically limited to diffusion-limited, and what happened in the first 1.9 min before the diffusion-limited process applied? The answer to these two questions lies in the differences in the interfacial properties between Ni and  $\text{In}_{0.53}\text{Ga}_{0.47}\text{As}$ . In the second type of specimen, an intermixing layer readily formed upon Ni deposition,

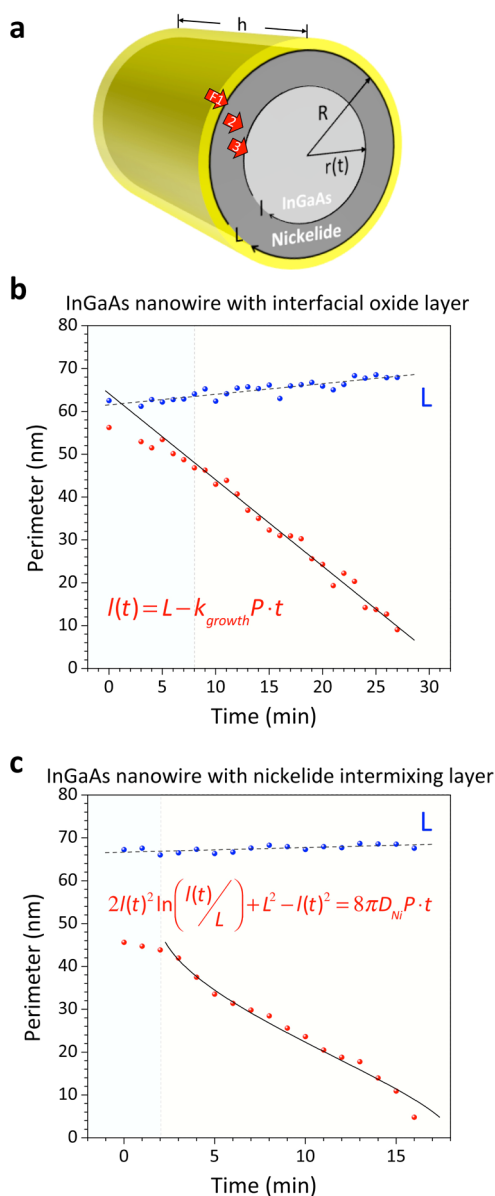


**Figure 4.** Modeling the formation of radial contact alloys. (a) A generalized model for metallic contact formation in the radial direction of a nanowire channel. The metal source is assumed to be unlimited, and the inner and outer perimeters of the reacted regions are labeled with  $l$  and  $L$ , respectively. (b) Plot of the inner and outer perimeters for the specimen that had an interfacial oxide layer, exhibiting a linear dependence with time and indicating a kinetically limited reaction process. (c) Plot of the inner and outer perimeters for the specimen that had no interfacial oxide layer but exhibited an intermixed surface region, with fits that corresponded to a mass-transport limited process.

resulting in a rounded  $\text{In}_{0.53}\text{Ga}_{0.47}\text{As}$  cross-section (Figure 3b,  $t = 0$ ). The rounded surfaces introduced many kink sites on small steps of nickelide/ $\text{In}_{0.53}\text{Ga}_{0.47}\text{As}$  interfaces, facilitating the reaction rate at these interfaces and thereby accelerating the kinetics of the reaction. The rate of arrival of Ni adatoms to the reaction interface became the rate-limiting step and therefore, the nickelide reaction became mass-transport/thermodynamically limited. It is also worth noting that the initial intermixing layer during metal deposition may not reach an equilibrium concentration (solubility limit) of Ni in  $\text{In}_{0.53}\text{Ga}_{0.47}\text{As}$ . Upon in situ heating the sample to 180 °C, Ni must first diffuse through

the intermixing layer and reach a point that exceeds the equilibrium concentration within this intermixing layer before Ni supersaturates the interface and nucleation and growth of a nickelide layer can proceed. This is corroborated by the experimentally observed subtle changes in  $l$  during the first 2 min (first three red data points in Figure 4c) that became rapid afterward. We extracted from the fits of the data from Figure 2c an  $L' = 51.3$  nm which agreed with the unreacted perimeter before the in situ experiment started (excluding the intermixing layer), and an effective diffusion coefficient ( $8\pi D_{\text{Ni}}P$ ) of 161.4  $\text{nm}^2/\text{min}$ , which is consistent with the volume diffusion coefficient that can be extracted from an Arrhenius plot in our previous study.<sup>28</sup> For  $t > 14$  min, the measured  $l$  of the unreacted  $\text{In}_{0.53}\text{Ga}_{0.47}\text{As}$  region fell more quickly than the fitting curve presumably due to interference from surface diffusion of the Ni on the imaging plane which reduced the image contrast of the crystalline core underneath.

During the above in situ heating experiments, we found that the nickelide reaction resulted in an amorphous phase in the nanowire cross sections throughout a wide range of reaction temperatures (180–350 °C). Interestingly, when the temperature was elevated to above 375 °C, the amorphized nickelide phase regrew slowly into a crystalline nickelide phase (Figure 5a). During this regrowth, polycrystallites were observed in the first 5 min followed by a well-aligned single-crystalline nickelide phase that appeared at the top-left corner. At later stages of crystallization, this single-crystalline nickelide phase seeded the regrowth from top-left corner downward into the cross-section of the nanowire and then from left side to the right until recrystallizing the entire nanowire cross-section. This crystalline nickelide phase was found to be  $\text{Ni}_2\text{In}_{0.53}\text{Ga}_{0.47}\text{As}$  by examining the lattice constant (Figure 5b) with a known value for this phase.<sup>28</sup> The regrown area of single crystalline  $\text{Ni}_2\text{In}_{0.53}\text{Ga}_{0.47}\text{As}$  versus the entire nanowire cross-sectional area was plotted as a function of time in Figure 5c. We found that the area transition from amorphous to crystalline nickelide can be fit with the Avrami equation,<sup>31</sup>  $Y = 1 - \exp(-Kt^n)$ , with  $n = 3.92$ , which is close to  $n = 4$  that is typical for an ideal homogeneous phase transformation.<sup>32</sup> Using energy dispersive spectroscopy (EDS) measurements, we found that the Ni concentration at the center of nanowire cross-section increased by 1.6 times after the crystalline regrowth. We hypothesize that, during the amorphization step, Ni diffused into the tetrahedral interstitial sites of the  $\text{In}_{0.53}\text{Ga}_{0.47}\text{As}$  lattice and formed a metastable nickelide phase (the lattice structure is shown in Figure S6 in the SI). This is in agreement with the fact that nickelide reacts faster on {110} facets than on {111} or {100} type of facets, as  $\langle 110 \rangle$  are usually the net crystal directions for interstitial diffusion.<sup>33</sup> During the crystalline regrowth step, further Ni was supplied from the surrounding contact, gradually forming the thermally stable  $\text{Ni}_2\text{In}_{0.53}\text{Ga}_{0.47}\text{As}$  phase. Given the shadowing effects during Ni deposition and nonconformal Ni coating (Figure 1 and Figure 3) as well as the thin FIB lamellae examined here, void formation on the sidewall of the reacted nanowire was unavoidable but can be resolved with conformal coating and wider Ni contacts.

In summary, we report the first direct observation of solid-state reaction dynamics between a metal (Ni) and a semiconductor ( $\text{In}_{0.53}\text{Ga}_{0.47}\text{As}$ ) nanowire along its cross-section. At typical temperatures at which the crystalline  $\text{Ni}_2\text{In}_{0.53}\text{Ga}_{0.47}\text{As}$  phase grows on planar  $\text{In}_{0.53}\text{Ga}_{0.47}\text{As}$  surfaces, the nanowire cross-section experienced a solid-state amorphization step and forms  $\text{Ni}_x\text{In}_{0.53}\text{Ga}_{0.47}\text{As}$  ( $x < 2$ ). During this

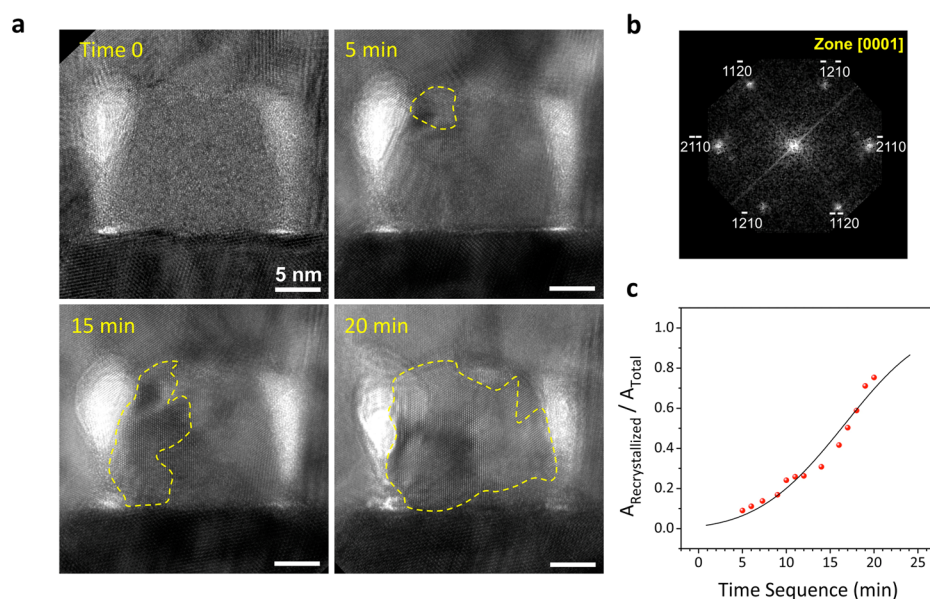


**Figure 5.** Recrystallization at elevated temperature. (a) High-resolution TEM sequences extracted from [Movie S3](#) in the SI during the in situ heating at 375 °C. The  $\text{In}_{0.53}\text{Ga}_{0.47}\text{As}$  nanowire has fully reacted with Ni to form an amorphous nickelide phase at 180 °C. During the recrystallization growth, well-aligned  $\text{Ni}_2\text{In}_{0.53}\text{Ga}_{0.47}\text{As}$  phase starts to form at the top-left corner, extends downward and then to the right, and finally recrystallizes the entire nanowire cross-section. (b) FFT image of the corresponding  $\text{Ni}_2\text{In}_{0.53}\text{Ga}_{0.47}\text{As}$  crystal, showing the diffraction pattern along the  $[0001]$  zone axis (projecting direction in TEM). (c) Plot of the area fraction of the recrystallized region over the entire cross sections as a function of time following the Avrami equation (see text).

amorphization process, nickelide reacts in a layer-by-layer manner proceeding by ledge movements on  $\{111\}$  facets along  $\langle 112 \rangle$  directions. Nickelide ledge movement events were recorded with time-sequenced high-resolution TEM images. These show that the phase transformation occurs through the evolution of stepped edges on non- $\{111\}$  facets and their consequent elimination resulted in an equilateral rhombus-like region bounded by  $\{111\}$  planes. The interface between Ni and the  $\text{In}_{0.53}\text{Ga}_{0.47}\text{As}$  nanowire was found to significantly influence the reaction kinetics and was captured by a model that we developed specifically for the cross-sectional geometry of nanowire channels. Finally, the amorphous  $\text{Ni}_x\text{In}_{0.53}\text{Ga}_{0.47}\text{As}$  ( $x < 2$ ) phase regrew into a single crystalline  $\text{Ni}_2\text{In}_{0.53}\text{Ga}_{0.47}\text{As}$  phase at temperatures above 375 °C by the additional incorporation of Ni adatoms from the contact reservoir. Overall, the results presented here provide a general guide for the development of crystalline, self-aligned contacts in nanoscale channels and can be generalized to radial reactions of metallic and other alloys into nanowire cross sections.

**Methods.** We used the FEI Tecnai F30 TEM and Aduro 300 double-tilt heating stage (Protochips Inc.) to perform the in situ heating experiments in this work. We operated TEM at 300 kV at the minimum electron dose that could still maintain clear imaging at highest magnification ( $\times 1$  M). The electron beam was never focused on the area of interest in order to minimize possible damage induced by electron beam. Digital video sequences were recorded at 3 frames/s, as the dynamic processes were slowed by well-chosen reaction temperatures. HRTEM images were extracted from the video frames and processed using the software package DigitalMicrograph where diffraction spots were masked and then inverted to enhance the image clarity. The compatible AHA thermal E-chips ( $\text{SiN}_x$  membranes, from Protochips Inc.) served as the heating platform for our experiments, on top of which a conductive ceramic membrane provided resistive heating and thermocou-

ple feedback temperatures to the controller. Temperatures in this paper were given by the readings on the controller with company-provided temperature calibration files for each thermal E-chip and through a comparison of reaction rates and morphologies with experiments performed ex situ where temperatures were measured using a thermocouple. We used a 1 °C/s ramping rate during the heating experiments, and the stage stabilized within 2 min after reaching the desired temperatures. To prepare our specimen on top of the thermal E-chips, we first fabricated the  $\text{In}_{0.53}\text{Ga}_{0.47}\text{As}$  nanowire structures with Ni contacts on a separate Si substrate (see [section I](#) of SI).<sup>28,34</sup> Then, we used the focused ion beam (FIB) to cut the lamellae specimen and in situ lift it out inside a SEM (FEI Nova 600) chamber. Finally, the lamellae was transferred on top of the membrane of a thermal E-chip horizontally, followed by further thinning of this lamellae until reaching e-beam transparency.

## ■ ASSOCIATED CONTENT

### 📄 Supporting Information

The Supporting Information is available free of charge on the ACS Publications website at DOI: [10.1021/acs.nanolett.6b04713](https://doi.org/10.1021/acs.nanolett.6b04713).

Details on the integration of FIB lamellae onto TEM platform, origin of the intermixing layer in between as-deposited Ni and InGaAs, derivation of the diffusion model in nanowire cross-section, in situ TEM results for InGaAs thin-film with interfacial oxide layer (PDF)

Movie S1: Solid-state amorphization process during Ni reaction with InGaAs nanowire crosssection that had a thin InGaAs surface oxide layer in between (AVI)

Movie S2: Solid-state amorphization process during Ni reaction with InGaAs nanowire crosssection that had a Ni-InGaAs intermixing layer in between before the reaction started (AVI)

Movie S3: Solid-state regrowth of the amorphous nickelide phase into well-aligned crystalline structure (AVI)

## AUTHOR INFORMATION

### Corresponding Author

\*E-mail: sdayeh@ucsd.edu.

### ORCID

Renjie Chen: 0000-0002-3145-6882

Shadi A. Dayeh: 0000-0002-1756-1774

### Author Contributions

R.C. and S.A.D. conceived and designed the research. R.C. performed the experiments and analyzed the data with S.A.D. who led all aspects of the project. K.L.J. and W.M.M. provided training, technical support, and discussions on in situ TEM operation. J.N. provided training, technical support, and discussions on dry etching of the nanowire structures. R.C. and S.A.D. wrote the manuscript, and all authors contributed to editing the manuscript.

### Notes

The authors declare no competing financial interest.

## ACKNOWLEDGMENTS

The fabrication and structural characterization were performed at the Center for Integrated Nanotechnologies (CINT), a U.S. Department of Energy Office of Basic Energy Sciences user facility at Los Alamos National Laboratory (Contract DE-AC52-06NA25396) and Sandia National Laboratories (Contract DE-AC04-94AL85000) through a CINT user proposal. The authors would like to acknowledge discussions with Drs. Nan Li, Wei Tang, Jinkyong Yoo, and Ms. Ren Liu, as well as discussions and technical support from Anthony R. James, Douglas V. Pete, Denise B. Webb, and Willard Ross of Sandia National Laboratories. S.A.D. thanks NSF support for R.C. under DMR-1503595 and partially from ECCS-1351980.

## REFERENCES

- Del Alamo, J. A. Nanometre-scale electronics with III-V compound semiconductors. *Nature* **2011**, *479*, 317–323.
- Cui, Y.; Lieber, C. M. Functional nanoscale electronic devices assembled using silicon nanowire building blocks. *Science* **2001**, *291*, 851–853.
- Duan, X.; Huang, Y.; Cui, Y.; Wang, J.; Lieber, C. M. Indium phosphide nanowires as building blocks for nanoscale electronic and optoelectronic devices. *Nature* **2001**, *409*, 66–69.
- Huang, Y.; Duan, X.; Wei, Q.; Lieber, C. M. Directed assembly of one-dimensional nanostructures into functional networks. *Science* **2001**, *291*, 630–633.
- Hisamoto, D.; et al. FinFET—a self-aligned double-gate MOSFET scalable to 20 nm. *IEEE Trans. Electron Devices* **2000**, *47*, 2320–2325.
- Ieong, M.; Doris, B.; Kedzierski, J.; Rim, K.; Yang, M. Silicon device scaling to the sub-10-nm regime. *Science* **2004**, *306*, 2057–2060.
- Ferain, I.; Colinge, C. A.; Colinge, J.-P. Multigate transistors as the future of classical metal-oxide-semiconductor field-effect transistors. *Nature* **2011**, *479*, 310–316.
- Wu, Y.; Xiang, J.; Yang, C.; Lu, W.; Lieber, C. M. Single-crystal metallic nanowires and metal/semiconductor nanowire heterostructures. *Nature* **2004**, *430*, 61–65.
- Léonard, F.; Talin, A. A. Electrical contacts to one- and two-dimensional nanomaterials. *Nat. Nanotechnol.* **2011**, *6*, 773–783.
- Tang, W.; Nguyen, B.-M.; Chen, R.; Dayeh, S. A. Solid-state reaction of nickel silicide and germanide contacts to semiconductor nanochannels. *Semicond. Sci. Technol.* **2014**, *29*, 054004.

(11) Appenzeller, J.; Knoch, J.; Tutuc, E.; Reuter, M.; Guha, S. Dual-gate silicon nanowire transistors with nickel silicide contacts. *Electron Devices Meeting (IEDM)* **2006**, 1–4.

(12) Chen, Y.; et al. Kinetic Manipulation of Silicide Phase Formation in Si Nanowire Templates. *Nano Lett.* **2013**, *13*, 3703–3708.

(13) Chen, Y.; et al. Kinetic Competition Model and Size-Dependent Phase Selection in 1-D Nanostructures. *Nano Lett.* **2012**, *12*, 3115–3120.

(14) Tang, J.; et al. Formation and device application of Ge nanowire heterostructures via rapid thermal annealing. *Adv. Mater. Sci. Eng.* **2011**, *2011*, 316513.

(15) Chueh, Y.-L.; et al. Formation and Characterization of Ni<sub>x</sub>InAs/InAs Nanowire Heterostructures by Solid Source Reaction. *Nano Lett.* **2008**, *8*, 4528–4533.

(16) Tang, W.; Dayeh, S. A.; Picraux, S. T.; Huang, J. Y.; Tu, K.-N. Ultrashort Channel Silicon Nanowire Transistors with Nickel Silicide Source/Drain Contacts. *Nano Lett.* **2012**, *12*, 3979–3985.

(17) Fauske, V. T.; et al. In Situ Heat-Induced Replacement of GaAs Nanowires by Au. *Nano Lett.* **2016**, *16*, 3051–3057.

(18) Tang, W.; et al. Nucleation and Atomic Layer Reaction in Nickel Silicide for Defect-Engineered Si Nanochannels. *Nano Lett.* **2013**, *13*, 2748–2753.

(19) Among the different compositions of these ternary phases (In<sub>x</sub>Ga<sub>1-x</sub>As), In<sub>0.53</sub>Ga<sub>0.47</sub>As is most commonly used, as it can be epitaxially grown on an InP substrate.

(20) Kim, S.; et al. Self-aligned metal source/drain In<sub>x</sub>Ga<sub>1-x</sub>As n-MOSFETs using Ni-InGaAs alloy. *Electron Devices Meeting (IEDM)*, 26.06.01–26.06.04, 2010.

(21) Zhang, X.; Guo, H. X.; Gong, X.; Zhou, Q.; Yeo, Y.-C. A Self-Aligned Ni-InGaAs Contact Technology for InGaAs Channel n-MOSFETs. *J. Electrochem. Soc.* **2012**, *159*, H511–H515.

(22) Abraham, M.; Yu, S.-Y.; Choi, W. H.; Lee, R. T.; Mohny, S. E. Very low resistance alloyed Ni-based ohmic contacts to InP-capped and uncapped n<sup>+</sup>-In<sub>0.53</sub>Ga<sub>0.47</sub>As. *J. Appl. Phys.* **2014**, *116*, 164506.

(23) Czornomaz, L.; et al. CMOS compatible self-aligned S/D regions for implant-free InGaAs MOSFETs. *Solid-State Electron.* **2012**, *74*, 71–76.

(24) Ivana. Crystal structure and epitaxial relationship of Ni<sub>4</sub>InGaAs<sub>2</sub> films formed on InGaAs by annealing. *J. Vac. Sci. Technol. B* **2013**, *31*, 012202.

(25) Shekhter, P.; Mehari, S.; Ritter, D.; Eizenberg, M. Epitaxial NiInGaAs formed by solid state reaction on In<sub>0.53</sub>Ga<sub>0.47</sub>As: Structural and chemical study. *J. Vac. Sci. Technol., B: Nanotechnol. Microelectron. Mater., Process., Meas., Phenom.* **2013**, *31*, 031205.

(26) Zhiou, S.; Rodriguez, P.; Gergaud, P.; Nemouchi, F.; Thanh, T. N. Influence of the substrate on the solid-state reaction of ultra-thin Ni film with a In<sub>0.53</sub>Ga<sub>0.47</sub>As under-layer by means of full 3D reciprocal space mapping. *2015 IEEE International Interconnect Technology Conference and 2015 IEEE Materials for Advanced Metallization Conference (IITC/MAM)*, 2015; pp 63–66.

(27) Ko, D. H.; Sinclair, R. Amorphous phase formation in an as-deposited platinum-GaAs interface. *Appl. Phys. Lett.* **1991**, *58*, 1851–1853.

(28) Chen, R.; Dayeh, S. A. Size and Orientation Effects on the Kinetics and Structure of Nickelide Contacts to InGaAs Fin Structures. *Nano Lett.* **2015**, *15*, 3770–3779.

(29) The atomic bilayer origins from the “zinc blend” structure of In<sub>x</sub>Ga<sub>1-x</sub>As lattice and means the coupled one layer of As atoms and one layer of In<sub>x</sub>Ga<sub>1-x</sub> atoms.

(30) Li, N.; Yadav, S. K.; Wang, J.; Liu, X.-Y.; Misra, A. Growth and Stress-induced Transformation of Zinc Blende AlN Layers in Al-AlN-TiN Multilayers. *Sci. Rep.* **2016**, *5*, 18554.

(31) Jena, A.; Chaturvedi, M. *Phase transformation in materials*; Prentice Hall, 1992.

(32) We believe that there exists no preferred heterogeneous nucleation site during this amorphous to crystalline regrowth such that  $n \sim 4$ . These polycrystallites formed over the entire NW cross-section

at the onset of the regrowth also referred to as homogeneous phase transformation.

(33) Edmonds, K.; et al. Mn Interstitial Diffusion in (Ga, Mn)As. *Phys. Rev. Lett.* **2004**, *92*, 037201.

(34) Dai, X.; Nguyen, B. M.; Hwang, Y.; Soci, C.; Dayeh, S. A. Novel heterogeneous integration technology of III–V layers and InGaAs finFETs to silicon. *Adv. Funct. Mater.* **2014**, *24*, 4420–4426.

# Supporting Information for

## Atomic Scale Dynamics of Contact Formation in the Cross-section of InGaAs Nanowire Channels

Renjie Chen,<sup>1</sup> Katherine L. Jungjohann,<sup>2</sup> William M. Mook,<sup>2</sup> John Nogan,<sup>2</sup> and Shadi A. Dayeh<sup>1,3,4</sup>□

<sup>1</sup> Department of Electrical and Computer Engineering, University of California San Diego, La Jolla, California 92093, USA

<sup>2</sup> Center for Integrated Nanotechnologies, Sandia National Laboratories, Albuquerque, New Mexico 87185, USA

<sup>3</sup> Materials Science and Engineering Program, University of California San Diego, La Jolla, California 92093, USA

<sup>4</sup> Department of NanoEngineering, University of California San Diego, La Jolla, California 92093, USA

□ email: sdayeh@ucsd.edu

### Table of Contents

<b>I. Integration of FIB lamellae onto TEM platform.....</b>	<b>2</b>
<b>II. Origin of the intermixing layer in between as-deposited Ni and InGaAs .....</b>	<b>5</b>
<b>III. Derivation of the diffusion model in nanowire cross-section .....</b>	<b>8</b>
<b>IV. In-situ TEM results for InGaAs thin-film with interfacial oxide layer .....</b>	<b>10</b>
<b>V. Lattice structure of nickelide phase.....</b>	<b>10</b>
<b>VI. List of supporting movies .....</b>	<b>10</b>
<b>References .....</b>	<b>11</b>

## I. Integration of FIB lamellae onto TEM platform

### (1) Fabrication of InGaAs nanowire channels on insulator on top of Si substrate

In this work, a 50nm-thin undoped  $\text{In}_{0.53}\text{Ga}_{0.47}\text{As}$  film (MBE grown on (001) InP by Intelligent Epitaxy Inc., Richardson, Texas) was first transferred on insulator on Si substrate with a solid-state wafer bonding process that we previously developed and reported elsewhere.<sup>1,2</sup> After the transfer, the stacking layers from top to bottom were 50nm  $\text{In}_{0.53}\text{Ga}_{0.47}\text{As}$ , 15nm  $\text{HfO}_2$ , 200nm  $\text{SiO}_2$ ,  $\text{NiSi}_x$  bonding layer (average thickness of  $\sim 200\text{nm}$ ), and  $500\mu\text{m}$  Si substrate. Secondly, the InGaAs layer was thinned down to  $\sim 20\text{nm}$  with 15 cycles of digital etching that is alternative oxidation with  $\text{O}_2$  plasma treatment (30W 3min), and oxide striping with diluted HCl solution (1:20 diluted in DI, dip for 2min). Thirdly, 20nm wide horizontal-lying nanowire structures were patterned on top of the  $\text{In}_{0.53}\text{Ga}_{0.47}\text{As}$  layer utilizing a 100 kV e-beam writer (JEOL JBX-6300FS) with beam size  $\sim 8\text{nm}$ . Negative e-beam resist, hydrogen silsesquioxane (HSQ FOx-16), was used as the etch mask for Ar-ion milling (Intlvac) to form the  $\text{In}_{0.53}\text{Ga}_{0.47}\text{As}$  nanowire channels. Ar-ion milling was chosen here instead of a chemical dry etch in order to achieve a straight nanowire sidewall. After the Ar-ion milling step, HSQ atop the nanowires was removed with three consecutive cycles of  $\text{O}_2$  plasma treatment and a short diluted HF dip, which also reduced the etch-induced surface damage and smoothed the InGaAs surface. This resulted in a nanowire channel cross-section with a squared shape, with an edge width of  $\sim 15\text{nm}$ . Finally, a 100nm Ni film was deposited onto two types of nanowire samples that were prepared with different surface treatments: (i) a thin layer of  $\text{In}_{0.53}\text{Ga}_{0.47}\text{As}$  surface oxide was intentionally introduced with  $\text{O}_2$  plasma treatment (30W 3min) before Ni deposition, and (ii) the  $\text{In}_{0.53}\text{Ga}_{0.47}\text{As}$  was dipped in diluted HCl solution and immediately loaded into electron-beam evaporator to prevent the formation of a native oxide layer. Type (i) specimen corresponds to the results shown in Figure 1&2 in the main text, and type (ii) specimen corresponds to the results shown in Figure 3.

To compare the interfacial properties of those two types of specimens after Ni deposition, another set of samples was prepared on a planar InGaAs film with identical interfacial treatments. As shown in Figure S1, both type (i) specimen (Fig. S1 a-c) and type (ii) specimen (Fig. S1 d-f) showed uniform interfaces over long range. With the interfacial oxide layer, the element Ni and InGaAs were separated sharply, while Ni and InGaAs were readily intermixed upon deposition at room temperature for the sample without the interfacial oxide layer. This can also be observed from elemental line-scans (Fig. S1 g-h) where the type (i) specimen had a sharp change of composition from Ni to InGaAs at the interface, and where the type (ii) specimen had a more graded change of composition from Ni to InGaAs. Inside the intermixing region, the Ni element maintained a

relatively smaller change in composition than that in the InGaAs film. This intermixing nickelide layer that is present for specimens without a interfacial oxide layer was caused by the latent heat during Ni condensation from vapor phase into solid phase as will be further discussed in section II.

## (2) Specimen lamellae preparation by focused-ion-beam (FIB) milling and in-situ lift-out (ILO)

TEM specimens in this work were prepared by FIB milling on the samples of InGaAs nanowire on insulator on Si substrate. Prior to FIB milling, 400nm SiO<sub>2</sub> and 50nm Pt were deposited atop the sample to prevent damage of interested area under ion beams. SiO<sub>2</sub> layer here was deposited at a low temperature (100 °C) plasma enhanced chemical vapor deposition (PECVD) process to prevent any possible reaction between Ni contact and InGaAs nanowires. The FIB and INLO process utilized here, shown in Figure S2 first row, follow conventional procedures,<sup>3,4</sup> in which a 30 kV Ga beam was used for rough milling and reduced voltage and current (10 kV, 0.1 nA) was used for fine milling.

## (3) Transferring specimen lamellae on top of thermal E-chips

The process to transfer FIB lamellae onto the TEM window of a thermal E-chip (AHA chip, Protochips Inc.) was shown in Figure S2, second row. The TEM window was made of conductive ceramic with many manmade circular holes for e-beam transparency. We intentionally drilled a larger rectangular hold for better imaging of our FIB lamellae for the HRTEM video recording of the reaction dynamics. We also deposited two 3 μm tall Pt posts on the edge of the opening region (shown in Fig. S2 step 5) to hold the transferred FIB lamellae. These two Pt posts not only helped maintaining the flatness of specimen lamellae during transfer, but also facilitated further thinning and cleaning steps by lifting up the lamellae from the surface of ceramic membrane. Finally, the transferred specimen lamellae was further thinned with FIB with reduced voltage and current (10 kV, 0.1 nA), until the lamellae reached a thickness ~ 60nm.

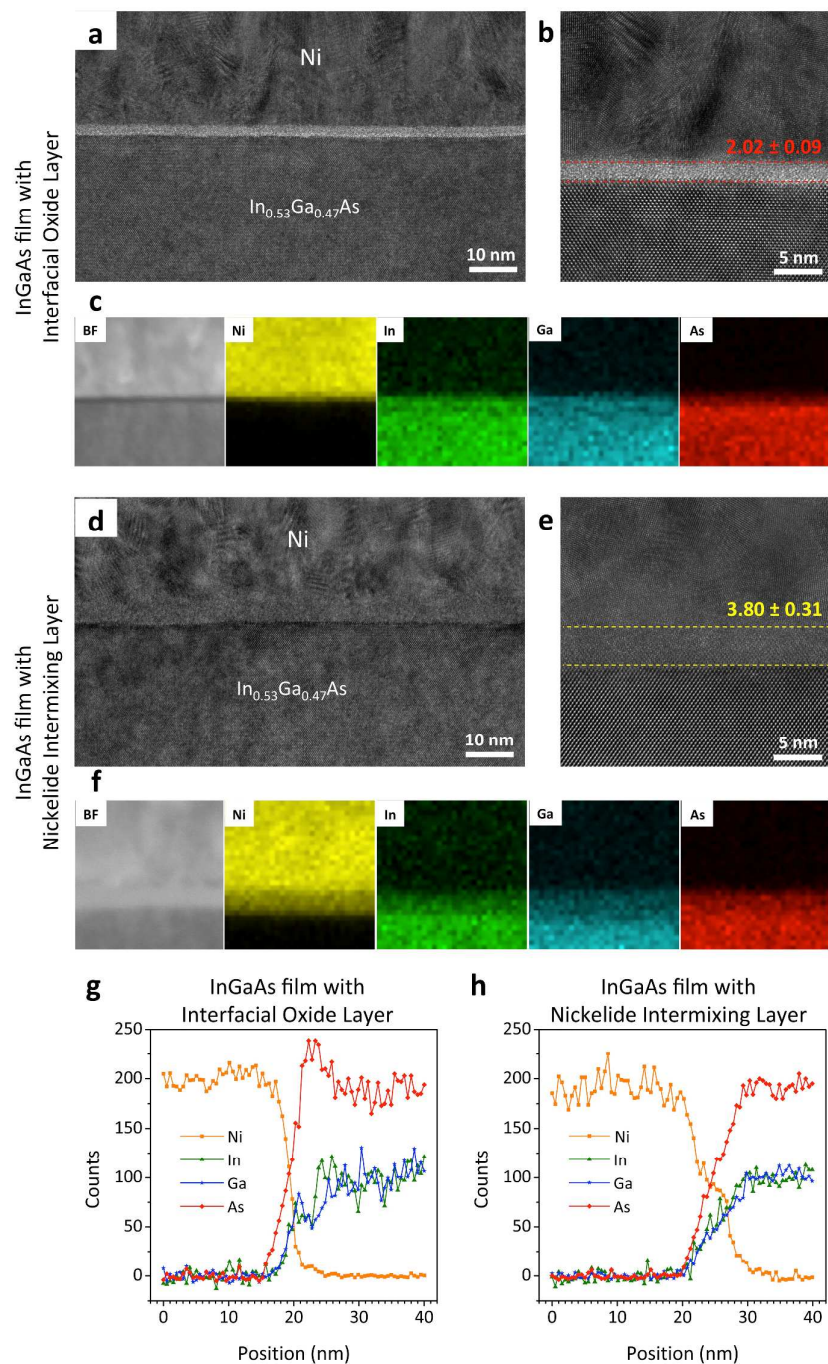


**Figure S1 | Comparison of interfacial structures for two types of specimens on InGaAs thin film. a-c,** TEM, HRTEM, and EDS mapping of type (i) specimen at the interface between Ni and InGaAs film. The light contrast layer at the interface, i.e. InGaAs surface oxide layer, has a uniform thickness of  $2.02 \pm 0.09$  nm. The EDS mapping of four elements show the sharp interface between Ni and InGaAs, indicating that the interfacial oxide layer effectively prevents the intermixing of Ni and InGaAs. **d-f,** TEM, HRTEM, and EDS mapping of type (ii) specimen at the interface between Ni and InGaAs film. The amorphous layer at the interface, i.e. Ni and InGaAs intermixing layer, has a uniform thickness of  $3.80 \pm 0.31$  nm. The EDS mapping of four elements show the clear evidence of intermixing between Ni and InGaAs at the interface. **g-h,** the EDS line-scan across the interface of type (i) and type (ii) specimens, respectively. Ni and As elemental counts are normalized according to their averaged top flats.

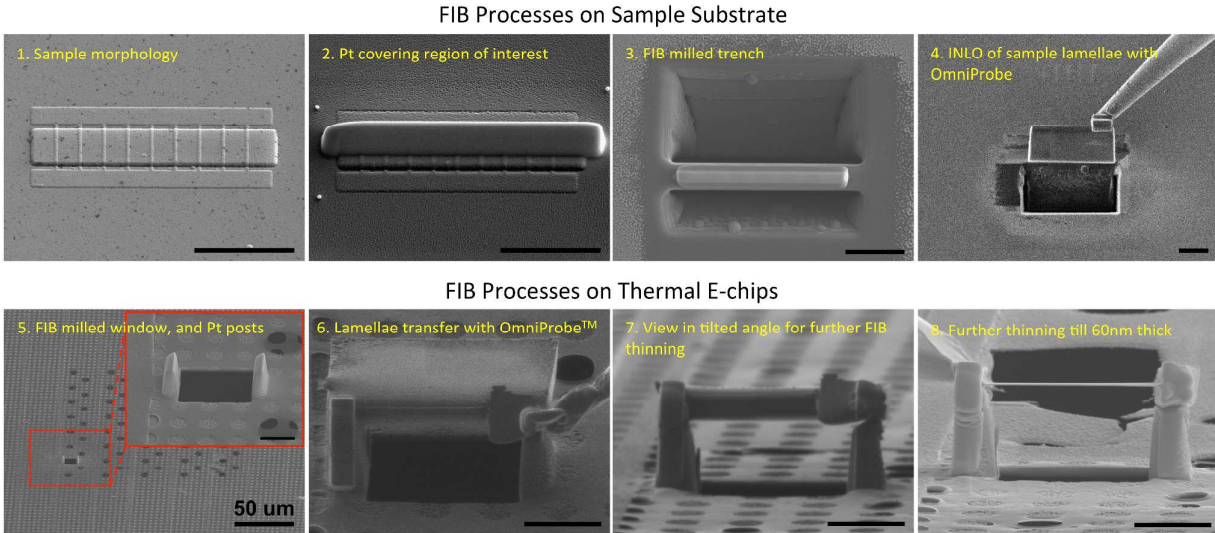


**Figure S2 | Sequences in FIB processes.** SEM images show the fabrication sequences to transfer the FIB cut lamellae from the home substrate onto the TEM membrane window of a thermal E-chip<sup>TM</sup>. All the scale bars are 5 $\mu$ m, except the one labeled separately in step 5.

## II. Origin of the intermixing layer in between as-deposited Ni and InGaAs

There are several possible reasons that may cause the intermixing between as-deposited Ni and InGaAs, including chamber overheating during evaporation, ion-beam-induced metal-semiconductor reaction,<sup>5,6</sup> or latent heat released from the condensation of metal atoms from vapor phase,<sup>7,8</sup> which we validated to be the cause below.

Firstly, we deposited the Ni in our experiments with an electron-beam evaporator with a total thickness of 100nm. Ni was deposited slowly (0.7  $\text{\AA}/\text{s}$ ) to prevent exaggerated stress and overheating, and the chamber was cooled down for 30min halfway after the deposition of the first 50nm of Ni. We also did a control experiment by depositing Ni by sputtering at room temperature where the surface pre-deposition treatments for InGaAs were similar to those samples that underwent electron-beam evaporation. The results are shown in Figure S3, with very similar interfacial structures as those with e-beam evaporated Ni, indicating that the Ni-InGaAs intermixing layer was not introduced by over-heating in the electron-beam evaporation chamber.

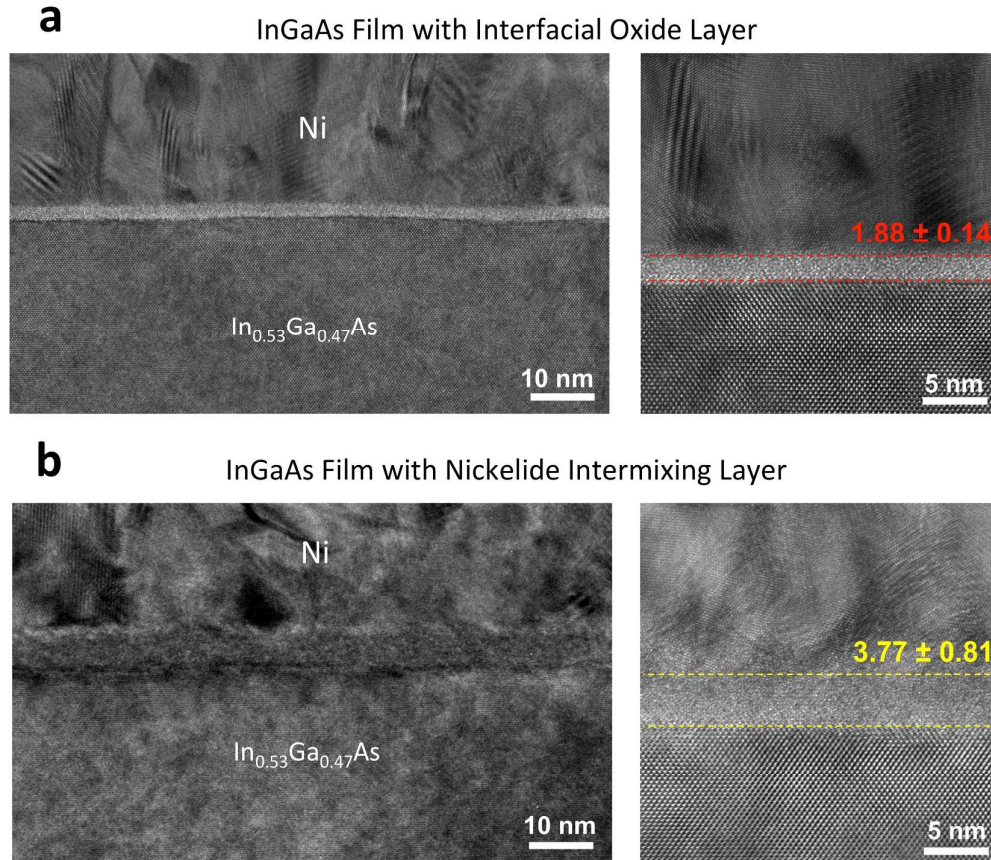


**Figure S3 | Comparison of interfacial structures when Ni deposited by sputtering.** **a**, TEM and HRTEM images of type (i) specimen at the interface between Ni and InGaAs film. The light contrast layer at the interface, i.e. InGaAs surface oxide layer, has a uniform thickness of  $1.88 \pm 0.14$  nm. **b**, TEM and HRTEM images of type (ii) specimen at the interface between Ni and InGaAs film. The amorphous layer at the interface, i.e. Ni and InGaAs intermixing layer, has a nearly uniform thickness of  $3.77 \pm 0.81$  nm.

Similarly, we excluded the possibility of ion-beam-induced metal-semiconductor reaction, also called ion-beam mixing, by processing FIB milling in a tilted angle (shown in Figure S4). Here, the Ni layer was deposited on two ends of InGaAs channel with HCl treated surface (no surface oxides present). After FIB milling, the interface structures were characterized under TEM. We found that the Ni-InGaAs intermixing layers were identical on both sides, and that both of them extended slightly out of the edge of Ni contacts. Ion-beam mixing is usually caused by penetrating energetic ions through the interface between a metal-film and semiconductor, overcoming equilibrium constraints in localized regions, and forcing atomic rearrangement, which will be localized and directional. This is contradictory to our observations here.

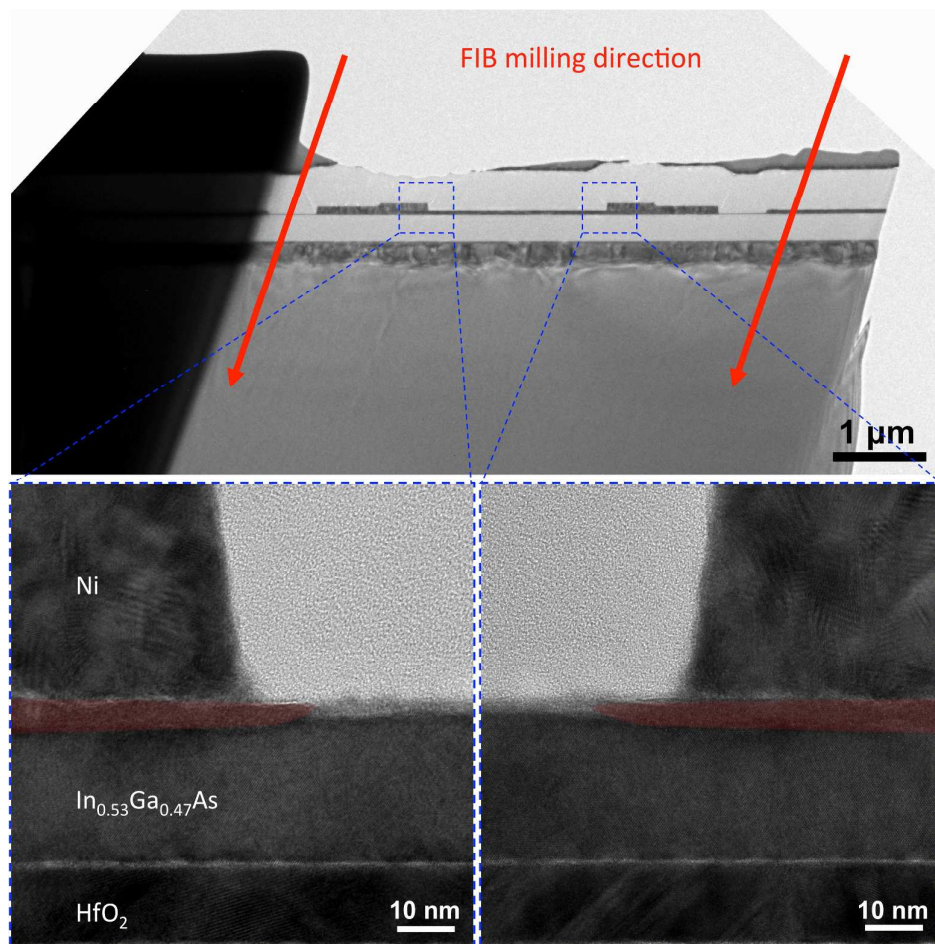


**Figure S4 | Interfacial structures when specimen is milled by FIB in a tilted angle.** TEM images of a type (ii) specimen in which Ni contacts were deposited at two ends of the InGaAs channel. The specimen was milled by FIB in a tilted angle in the direction of the red arrows in the top panel. Zoomed in TEM images show identical Ni-InGaAs intermixing layers on both sides, and both intermixing layers extended slightly out of the edge of Ni contacts. The evolution of the nickelide extended region to the right from the left contact indicates that the Ni-InGaAs intermixing is not introduced by the directional ion-beam induced mixing (directed to the left of the sample).

The third possibility is that the latent heat released from the condensation of metal atoms from vapor phase. In fact, when a metal and a semiconductor are brought in contact at room temperature, an intermixing layer can be readily formed between them due to the screening coulomb interaction by free electrons in the metal, which weakens the covalent bonding energy at the semiconductor surface.<sup>9,10</sup> However, the intermixing layer due to electron screening is usually a monolayer or two thick. It has been previously observed that the as-deposited metal on semiconductor can introduce thicker (few nanometers) amorphous intermixture caused by the negative heat (latent heat) from metal condensation. The amorphous interfacial layers between the deposited metal and semiconductor were also observed in other metal/III-V systems.<sup>11,12</sup>

### III. Derivation of the diffusion model in nanowire cross-section

The fluxes of Ni atoms in the three processes as shown in Figure 4, can be expressed as:

$$F_1 = k_{dissolve} (C_{Ni/Nickelide}^{eq} - C_R) \cdot 2\pi R h = k_{dissolve} (C_{Ni/Nickelide}^{eq} - C_R) \cdot hL \quad (S3.1)$$

$$F_2 = D_{Ni} (C_r - C_R) \cdot 2\pi h \cdot \left[ \ln\left(\frac{r(t)}{R}\right) \right]^{-1} = D_{Ni} (C_r - C_R) \cdot 2\pi h \cdot \left[ \ln\left(\frac{l(t)}{L}\right) \right]^{-1} \quad (S3.2)$$

$$F_3 = k_{growth} (C_r - C_{Nickelide/InGaAs}^{eq}) \cdot 2\pi r(t) h = k_{growth} (C_r - C_{Nickelide/InGaAs}^{eq}) \cdot hl(t) \quad (S3.3)$$

where  $k_{dissolve}$  and  $k_{growth}$  are the rate constants for Ni dissolution and nickelide growth respectively.

$C_{Ni/Nickelide}^{eq}$  and  $C_R$  represents the equilibrium and instant Ni concentrations across the Ni/nickelide interface.  $C_r$  and  $C_{Nickelide/InGaAs}^{eq}$  denotes the instant and equilibrium Ni concentrations across the nickelide/In<sub>0.53</sub>Ga<sub>0.47</sub>As interface.

#### Derivation of equation F<sub>2</sub>:

Considering Fick's first law of diffusion in cylindrical coordinates, we can write:

$$\vec{J} = -D \frac{dC}{dr} \vec{r}.$$

The Ni atomic flux can be expressed as  $F = D \frac{dC}{dr} \cdot 2\pi r h$ , pointing to the core.

Integration of the equation  $\frac{F}{2\pi r h \cdot D} dr = dC$  across the entire nickelide region yields:

$$\int_R^r \frac{F}{2\pi r h \cdot D} dr = \int_{C_R}^{C_r} dC$$

Therefore, we can write:

$$\frac{F}{2\pi h \cdot D} \ln\left(\frac{r}{R}\right) = C_r - C_R, \Rightarrow F = D(C_r - C_R) \cdot 2\pi h \cdot \left[ \ln\left(\frac{r}{R}\right) \right]^{-1}$$

Under steady state condition,  $F_1=F_2=F_3=F$ , we can obtain a characteristic equation of the reaction as follows:

$$F = k_{dissolve} (C_{Ni/Nickelide}^{eq} - C_R) \cdot hL = D_{Ni} (C_r - C_R) \cdot 2\pi h \cdot \left[ \ln\left(\frac{l(t)}{L}\right) \right]^{-1} = k_{growth} (C_r - C_{Nickelide/InGaAs}^{eq}) \cdot hl(t), \quad (S3.4)$$

hence:

$$F = \frac{C_{Ni/Nickelide}^{eq} - C_{Nickelide/InGaAs}^{eq}}{\frac{1}{k_{dissolve} \cdot hL} - \frac{\ln\left(\frac{l(t)}{L}\right)}{D_{Ni} \cdot 2\pi h} + \frac{1}{k_{growth} \cdot hl(t)}}. \quad (S3.5)$$

Because of mass conservation,  $F \cdot \frac{M_{\text{Nickelide}}}{N_A \cdot \rho_{\text{Nickelide}}} = -2\pi r(t)h \cdot \frac{dr(t)}{dt} = -\frac{hl(t)}{2\pi} \cdot \frac{dl(t)}{dt}$  (S3.6)

and assuming that  $P = \frac{2\pi M_{\text{Nickelide}}}{N_A \cdot \rho_{\text{Nickelide}}} \cdot (C_{\text{Ni/Nickelide}}^{\text{eq}} - C_{\text{Nickelide/InGaAs}}^{\text{eq}})$  (S3.7)

we can write,

$$\frac{dl(t)}{dt} = -\frac{P}{\frac{l(t)}{k_{\text{dissolve}}L} - \frac{l(t) \cdot \ln\left(\frac{l(t)}{L}\right)}{2\pi D_{\text{Ni}}} + \frac{1}{k_{\text{growth}}}} \quad (\text{S3.8})$$

Here, the three terms in the denominator represent three rate-limiting mechanisms. If these three rate-limiting mechanisms are separately considered, the differential equation can be solved.

(i) If Ni dissolution at the Ni/nickelide interface is the rate-limiting step, we obtain:

$$\frac{dl(t)}{dt} \approx -\frac{P \cdot k_{\text{dissolve}}L}{l(t)}, \quad \text{therefore: } l(t) = \sqrt{L^2 - 2k_{\text{dissolve}}LP \cdot t}. \quad (\text{S3.9})$$

(ii) If nickelide growth at the nickelide/InGaAs interface is the rate-limiting step, we obtain:

$$\frac{dl(t)}{dt} \approx -P \cdot k_{\text{growth}}, \quad \text{therefore: } l(t) = L - k_{\text{growth}}P \cdot t. \quad (\text{S3.10})$$

(iii) If the Ni diffusion in the reacted nickelide region is the rate-limiting step, we obtain:

$$\frac{dl(t)}{dt} \approx P \cdot \frac{2\pi D_{\text{Ni}}}{l(t) \cdot \ln\left(\frac{l(t)}{L}\right)}, \quad \text{therefore: } 2l(t)^2 \ln\left(\frac{l(t)}{L}\right) + L^2 - l(t)^2 = 8\pi D_{\text{Ni}}P \cdot t. \quad (\text{S3.11})$$

#### Solution of the Differential equation S3.11:

To solve the equation  $l(t) \cdot \ln\left(\frac{l(t)}{L}\right) dl(t) = 2\pi D_{\text{Ni}}P dt$ ,

we can assume  $y = \frac{l(t)}{L}$ , and then obtain  $L^2 y \ln y dy = 2\pi D_{\text{Ni}}P dt$ .

We then perform integration of this equation across the entire nickelide region:

$$\int_1^{l/L} L^2 y \ln y dy = \int_0^t 2\pi D_{\text{Ni}}P dt$$

Using known integrals for logarithmic functions,  $\int x \ln x dx = x^2 \left(\frac{\ln x}{2} - \frac{1}{4}\right)$ , we obtain:

$$L^2 y^2 \left(\frac{\ln y}{2} - \frac{1}{4}\right) \Big|_1^{l/L} = 2\pi D_{\text{Ni}}P \cdot t, \Rightarrow 2l(t)^2 \ln\left(\frac{l(t)}{L}\right) + L^2 - l(t)^2 = 8\pi D_{\text{Ni}}P \cdot t. \text{ We utilize this}$$

equation in the fits of Fig. 4c of the main text.

#### IV. In-situ TEM results for InGaAs thin-film with interfacial oxide layer

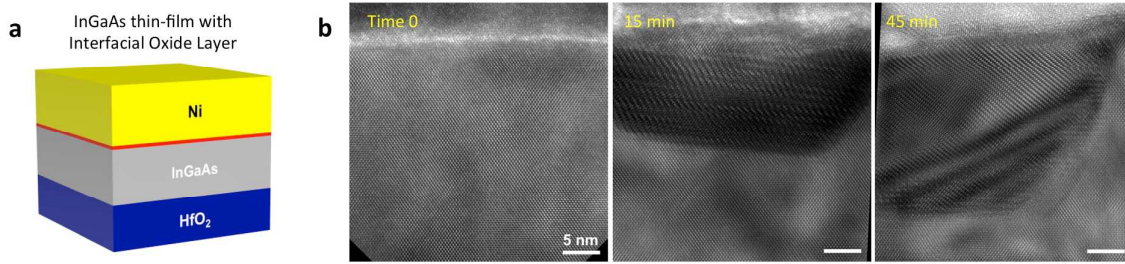


**Figure S5 | In-situ heating TEM results for  $\text{In}_{0.53}\text{Ga}_{0.47}\text{As}$  thin film sample.** **a**, schematic image shows the stacking of Ni on planar InGaAs film with a thin InGaAs oxide layer at the interface. **b**, the time sequenced HRTEM images of the in-situ heating experiment performed at 290 °C. At time 0, the Ni contact was separated from InGaAs by the surface oxide layer. Then, Ni gradually diffused into InGaAs and formed crystalline nickelide phase without transitioning through an amorphization step. In the first 15min, the nickelide structure was polycrystalline with overlapped grains forming moiré pattern. Beyond 15min and up to the end of recording time of 45min, the slightly misaligned polycrystalline nickelide gradually transferred into single crystalline structure directly under the nickel contact.

#### V. Lattice structure of nickelide phase

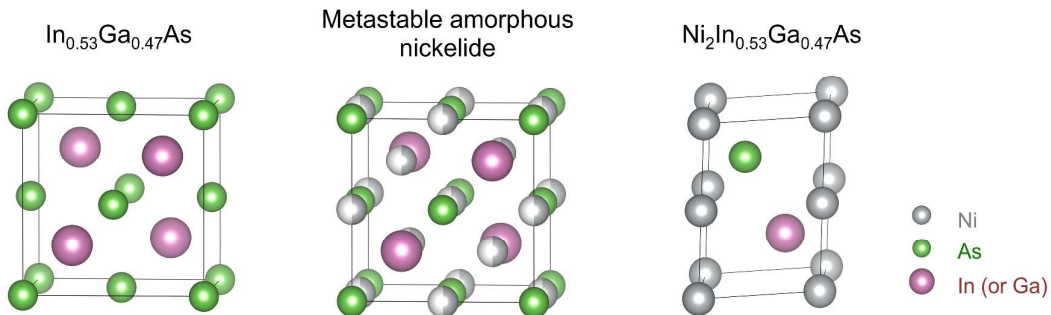


**Figure S6 | Lattice structures of pristine  $\text{In}_{0.53}\text{Ga}_{0.47}\text{As}$ , metastable amorphous nickelide phase, and crystalline  $\text{Ni}_2\text{In}_{0.53}\text{Ga}_{0.47}\text{As}$  phase.** Non-reacted  $\text{In}_{0.53}\text{Ga}_{0.47}\text{As}$  has the zinc-blende structure with lattice constant of  $a = 5.87 \text{ \AA}$ . During the amorphization step, we hypothesize that Ni diffused into the tetrahedral interstitial sites of the  $\text{In}_{0.53}\text{Ga}_{0.47}\text{As}$  lattice, occupied part of them and formed a metastable nickelide phase. The crystalline  $\text{Ni}_2\text{In}_{0.53}\text{Ga}_{0.47}\text{As}$  lattice is hexagonal and adopts the NiAs (B8) structure with lattice constants of  $a = 3.93 \text{ \AA}$ ,  $c = 5.10 \text{ \AA}$ .<sup>2</sup>

#### VI. List of supporting movies

**Movie S1:** Solid-state amorphization process during Ni reaction with InGaAs nanowire cross-section that had a thin InGaAs surface oxide layer in between. The reaction was recorded

at 180 °C. The frame rate is accelerated by 8 times.

**Movie S2:** Solid-state amorphization process during Ni reaction with InGaAs nanowire cross-section that had a Ni-InGaAs intermixing layer in between before the reaction started. The reaction was recoded at 180 °C. The frame rate is accelerated by 8 times.

**Movie S2:** Solid-state regrowth of the amorphous nickelide phase into well-aligned crystalline structure. The reaction was recoded at 375 °C. The frame rate is accelerated by 8 times. Scale bars in all movies are 2 nm.

## References

- 1 Dai, X., Nguyen, B. M., Hwang, Y., Soci, C. & Dayeh, S. A. Novel heterogeneous integration technology of III–V layers and InGaAs finFETs to silicon. *Advanced Functional Materials* **24**, 4420-4426 (2014).
- 2 Chen, R. & Dayeh, S. A. Size and Orientation Effects on the Kinetics and Structure of Nickelide Contacts to InGaAs Fin Structures. *Nano letters* **15**, 3770-3779 (2015).
- 3 Giannuzzi, L. A. *et al.* in *Introduction to focused ion beams* 201-228 (Springer, 2005).
- 4 Mayer, J., Giannuzzi, L. A., Kamino, T. & Michael, J. TEM sample preparation and FIB-induced damage. *Mrs Bulletin* **32**, 400-407 (2007).
- 5 Lau, S. *et al.* Ion-beam mixing of metal-semiconductor eutectic systems. *Nuclear Instruments and Methods* **182**, 97-105 (1981).
- 6 Nastasi, M. & Mayer, J. Ion beam mixing in metallic and semiconductor materials. *Materials Science and Engineering: R: Reports* **12**, 1-52 (1994).
- 7 Sands, T. *et al.* Ni, Pd, and Pt on GaAs: A comparative study of interfacial structures, compositions, and reacted film morphologies. *Journal of Materials Research* **2**, 262-275 (1987).
- 8 Ko, D. H. & Sinclair, R. Amorphous phase formation and initial interfacial reactions in the platinum/GaAs system. *Journal of applied physics* **72**, 2036-2042 (1992).
- 9 Hiraki, A., Shuto, K., Kim, S., Kammura, W. & Iwami, M. Room - temperature interfacial reaction in Au - semiconductor systems. *Applied Physics Letters* **31**, 611-612 (1977).
- 10 Hiraki, A. A Model on the Mechanism of Room Temperature Interfacial Intermixing Reaction in Various Metal - Semiconductor Couples: What Triggers the Reaction? *Journal of The Electrochemical Society* **127**, 2662-2665 (1980).
- 11 Sands, T., Keramidis, V., Washburn, J. & Gronsky, R. Structure and composition of NixGaAs. *Applied physics letters* **48**, 402-404 (1986).
- 12 Ko, D. H. & Sinclair, R. Amorphous phase formation in an as - deposited platinum - GaAs interface. *Applied physics letters* **58**, 1851-1853 (1991).